Available online at www.sciencedirect.com

SCIENCE DIRECT®

Thin Solid Films 467 (2004) 88–92

thin solid films

www.elsevier.com/locate/tsf

Reflectance and photoluminescence characterization of $Be_xZn_{1-x}Te$ epilayers

O. Maksimov[a,*], Martin Muñoz[b], N. Samarth[a], M.C. Tamargo[b]

[a] *Department of Physics, Pennsylvania State University, 104 Davey Lab, University Park, PA 16802, USA*
[b] *Department of Chemistry, City College of New York, New York, NY 10031, USA*

Received 28 November 2003; received in revised form 26 February 2004; accepted 2 March 2004
Available online 30 July 2004

Abstract

$Be_xZn_{1-x}Te$ thin films were grown on InP substrates by molecular beam epitaxy (MBE). Optical properties of the epilayers were studied using reflectance and photoluminescence (PL) measurements. An increase in the full width at half maximum of the emission line with the increase in BeTe content was observed and explained by the disorder-induced broadening. The temperature dependence of the band gap energy was determined from reflectance spectra and fitted by semiempirical equation taking into account average phonon energy and electron–phonon interaction. A reduction of the temperature variation of the band gap with the increase in BeTe content was observed. We propose that this effect is due to the decrease of the lattice contribution caused by the lattice hardening properties of BeTe.

PACS: 78.66.Hf; 78.40.Fy; 78.55.Et
Keywords: BeZnTe; Band gap; Photoluminescence; Reflectance; Molecular beam epitaxy

1. Introduction

$Be_xZn_{1-x}Te$ is a novel wide band gap semiconductor alloy that attracted much interest due to its possible application in optoelectronic devices. It can be grown with high crystalline quality on GaAs and InP substrates and can be doped p-type to carrier concentration levels in excess of 10^{19} cm^{-3} [1,2]. It was already successfully used as a cladding layer in the current injected laser diodes (LDs) operating at 560 nm [3]. It should be noted that it is difficult to obtain a lasing emission at this wavelength both from $Al_xGa_yIn_{1-x-y}N$ and $Al_xGa_yIn_{1-x-y}P$ LDs [4,5]. Also, since $Be_xZn_{1-x}Te$ band gap can be tuned from 2.8 to 4.1 eV, by adjusting BeTe content, it can be used as a transparent conductive electrode in multi junction tandem solar cells and short wavelength photo detectors.

Room temperature optical studies of $Be_xZn_{1-x}Te$ alloy analyzed compositional dependence of the different band gaps and showed that it undergoes a transition from direct to indirect band gap at $x \sim 0.28$ [6–8]. However, temperature dependence of the band gap energy is unknown. Meanwhile, this information is useful for the optimization of the design of quantum well lasers. Because of the high resistivity of the active region, self-heating occurs during the operation of LDs. If the band offsets depend on temperature, a decrease in the quantum confinement can occur, causing carrier leakage. This will reduce the spectral gain, increasing the laser threshold and decreasing the lifetime of the device. Temperature stability is also important for the devices operating in the extreme environmental conditions, like solar cells installed at space stations or satellites where the operation temperature varies from 150 °C (at the sun shining side) to −150 °C (at the dark side).

In this article, we report the use of photoluminescence (PL) and reflectance spectroscopies to study optical properties of epilayers grown by molecular beam epitaxy (MBE) on InP substrates. A significant emission line broadening with increase in BeTe content is observed and explained by the increase in the alloy disorder. The temperature dependence of the band gap energy is determined from reflectance spectra and modeled by a three-parameter fit developed by

* Corresponding author. Tel.: +1-814-863-9514; fax: +1-814-865-3604.
E-mail address: Maksimov@netzero.net (O. Maksimov).

0040-6090/$ - see front matter © 2004 Elsevier B.V. All rights reserved.
doi:10.1016/j.tsf.2004.03.003

O'Donnell and Chen [9]. It is determined that temperature dependence of $Be_xZn_{1-x}Te$ band gap is decreasing with the increase in Be content and is smaller compared to other wide band gap semiconductors, making it preferable alloy for device application.

2. Experimental details

$Be_xZn_{1-x}Te$ epilayers were grown in a Riber 2300P MBE system using elemental Be, Zn, and Te sources. This system consists of two growth chambers connected by an ultra-high vacuum transfer channel. One growth chamber is used for As-based III–V materials and the other is for wide band gap II–VI materials.

The growth was performed on semi-insulating InP (100) substrates. The substrates were deoxidized in the III–V chamber by heating to 480 °C with an As flux impinging on the InP surface. A lattice matched $In_{0.53}Ga_{0.47}As$ buffer layer (170 nm) was grown after the deoxidization. The buffer layer was terminated with an As-rich (2×4) surface reconstruction. Then, the samples were transferred in vacuum to the II–VI chamber for the $Be_xZn_{1-x}Te$ growth. $Be_xZn_{1-x}Te$ layers were grown at 270 °C under Te-rich conditions, as characterized by a (2×1) surface reconstruction [10], with a group VI to group II flux ratio of ~3. The growth rate was around 0.25–0.45 μm/h and the layers were 0.5–0.9 μm thick.

The growth mode and surface reconstruction were monitored in situ by reflection high-energy electron diffraction. Lattice constants were measured by single-crystal and double-crystal X-ray diffraction using Cu $K_{\alpha 1}$ radiation. Alloy composition was estimated from the lattice constant, assuming the validity of Vegard's law and using 6.103 and 5.617 Å as the lattice constants for ZnTe and BeTe, respectively [11]. The surface morphology was investigated using a contact mode atomic force microscope. The measurements were performed at the scan rate of 1–2 Hz with SiN tips. PL measurements were performed in a liquid He continuous flow cryostat at 4.2 K. The 325-nm line of a He–Cd laser was used for excitation. The collected PL was spectrally resolved by a monochromator and detected by a photo multiplier tube. Reflectance measurements were performed in the same cryostat in the temperature range from 4.2 to 300 K using a 200-W Hg lamp.

3. Results and discussion

PL and reflectivity spectra at 4.2 K for the samples grown are shown in Fig. 1 by the solid and dotted lines, respectively. The quenching of Fabry-Perot oscillations in the reflectance spectra corresponds to the onset of interband absorption and is identified as the Γ→Γ direct band gap. The energy of $Be_xZn_{1-x}Te$ direct band gap increases with

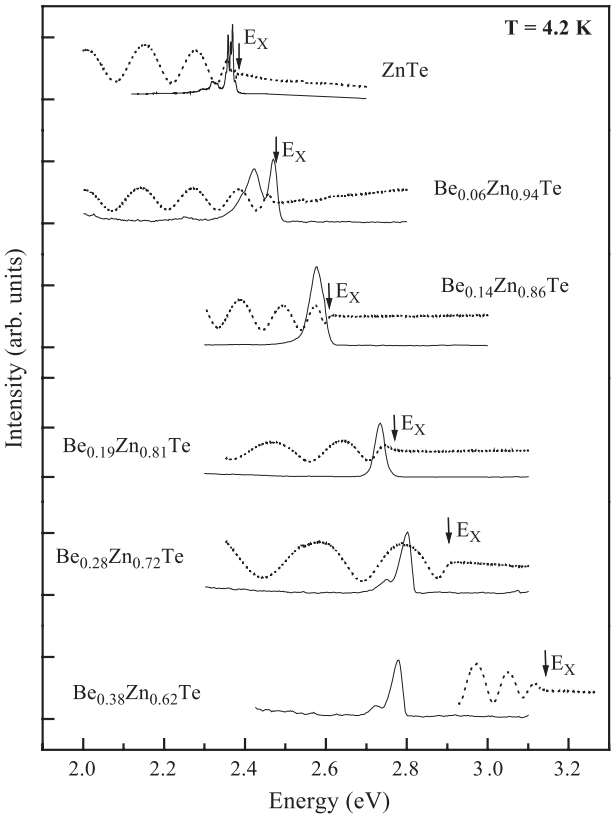

Fig. 1. Photoluminescence (solid line) and reflectance (dotted line) spectra of $Be_xZn_{1-x}Te$ epilayers at 4.2 K.

increase in BeTe content (x). This change is nearly linear (18 meV for 1% of BeTe) and no band gap bowing is observed. Since $Be_xZn_{1-x}Te$ is a common anion system, we expect that the observed increase in the band gap energy is mostly due to the rise of the conduction band.

$Be_xZn_{1-x}Te$ PL spectra are dominated by bound exciton emission lines. In several spectra, a second, usually weak peak is present at lower energy, about 50 meV below the high-energy peak. This peak is probably due to the defect or impurity related emission. For $Be_xZn_{1-x}Te$ alloys with $x<0.28$, Stokes shift between the PL peak energy and the band gap measured through reflectivity measurements is very small (on the order of a few meV s). When BeTe content exceeds 28%, Stokes shift increases significantly and exceeds 300 meV for $Be_{038}Zn_{0.62}Te$. This is due to the direct-to-indirect transition in $Be_xZn_{1-x}Te$ with $x \sim 0.28$.

A significant broadening of the emission line with the increase in BeTe content is observed, as shown in Fig. 2 by open symbols. Usually, the broadening of the emission line is due to the decrease in the crystalline quality of the epilayers or increase in the alloy disorder. In this case, the crystalline quality is increasing with the BeTe content since the lattice mismatch to InP substrate is decreasing. For example, the $Be_{0.46}Zn_{0.54}Te$ epilayer, that is closely lattice matched to InP substrate ($\Delta a/a$=0.17%), demonstrates a narrow X-ray rocking curve with a full width at half

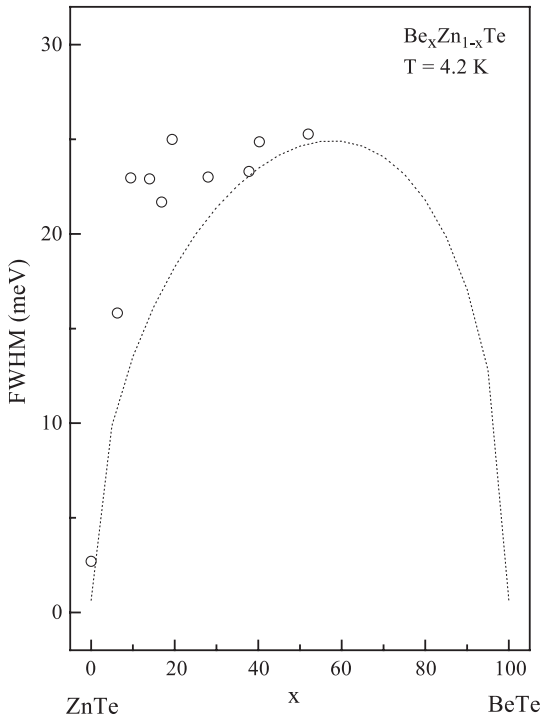

Fig. 2. Full width at half maximum of exciton emission line width of $Be_xZn_{1-x}Te$ epilayers as function of the composition. Open symbols are experimental data and dotted line is a theoretical fit.

maximum (FWHM) of ~72 arc s, as shown in Fig. 3 and exhibits good surface morphology with a root mean square roughness of ~1.4 nm, as shown in Fig. 4. Low defect density of 5×10^5 cm^{-2} is also measured by etch pit density measurements. These results are comparable to the reported for ZnSe epilayers grown on GaAs [12].

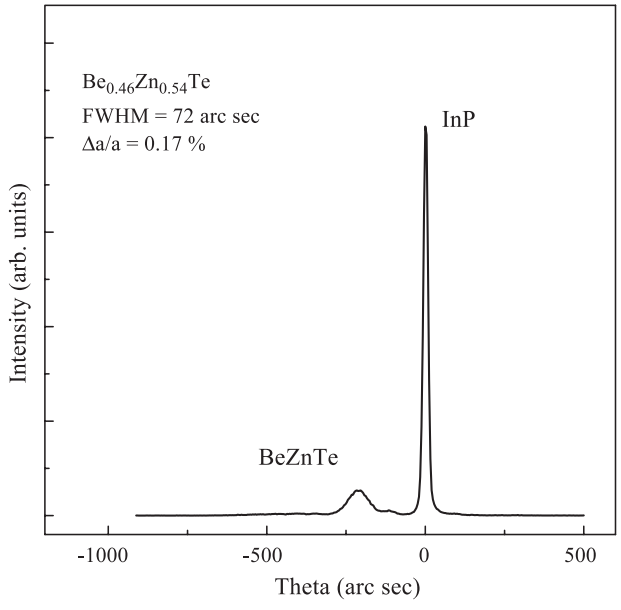

Fig. 3. (004) X-ray rocking curve for a $Be_{0.46}Zn_{0.54}Te$ epilayer grown on InP substrate.

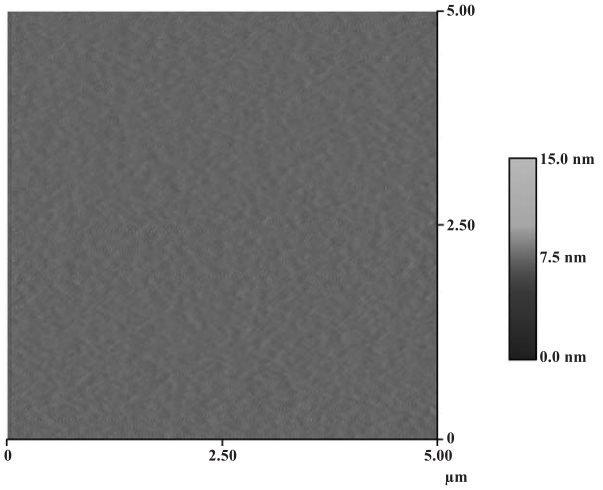

Fig. 4. Atomic force micrograph for a $Be_{0.46}Zn_{0.54}Te$ epilayer.

We explain emission line broadening by the increase in the statistical alloy disorder. The standard deviation of the alloy composition in $A_xB_{1-x}C$ alloy (σ_x) is described by a binomial (Bernoulli) distribution:

$$\sigma_x = [x(1-x)/KV_{\mathrm{exc}}]^{1/2} \quad (1)$$

where K is the cation density and V_{exc} is the volume of an exciton. Since there are four cations in the unit cell of zinc—blend crystal lattice with lattice constant a_0, cation density is:

$$K = 4a_0^{-3} \quad (2)$$

The volume of an exciton is:

$$V_{\mathrm{exc}} = (4/3)\pi r_{\mathrm{B}}^3 \quad (3)$$

where r_{B} is the Bohr radius of exciton. The Bohr radius of exciton in ZnTe is ~5.2 nm [11] while that in BeTe is unknown. Since dielectric constant of BeTe is ~25% smaller than that of ZnTe [13], we expect the exciton Bohr radius to be also smaller by 25%.

The broadening of an exciton line (σ_{exc}) due to the deviation of the alloy composition is given by an equation [14]:

$$\sigma_{\mathrm{exc}} = 2(2\ln(2))^{1/2}(\mathrm{d}E_{\mathrm{g}}/\mathrm{d}x)\sigma_x \quad (4)$$

and the FWHM of the emission line is expressed as a sum of thermal emission broadening ($1.8\ k_{\mathrm{B}}T$) and σ_{exc}. The FWHM fit that considers these contributions is shown in Fig. 2 by dotted line. It estimates an emission line width for an ideal solution and does not take into account broadening due to the inferior crystal quality, alloy clustering, and defects. Therefore, it is expected to be narrower then the real line widths. However, a good correlation

between experimentally measured emission line widths and theoretically estimated is observed, especially for the epilayers with higher BeTe content that have high crystalline quality.

The temperature dependence of the direct band gap was studied for the epilayers with BeTe content up to 38% by reflectance measurements. The data are shown in Fig. 5 by open symbols. At 4.2 K, the band edge absorption for ZnTe epilayer is at 2.381 eV, slightly below ZnTe band gap [11]. The difference is equal to the exciton binding energy (13 meV) suggesting that excitonic absorption (E_X) dominates the spectrum.

As the temperature increases, the transition point exhibits a red shift due to the decrease in the band gap energy that is caused by the electron–phonon interactions and lattice dilation. The one-electron theory of electron energy bands of crystalline solids is based on the assumption that crystal is a perfectly periodic structure. This assumption is correct only at absolute zero. At finite temperatures, interactions between electrons and phonons change electron energy, changing energy of the gap with temperature. Expansion of the crystal lattice with temperature reduces the overlap between the electronic wave functions of the neighboring atoms and reduces band gap energy. However, lattice contribution to the band gap shift is smaller than contribution from the electron–phonon interactions.

A number of semi-empirical equations exist that describe temperature dependence of band gap energy with different level of success. We fit the temperature behavior of the

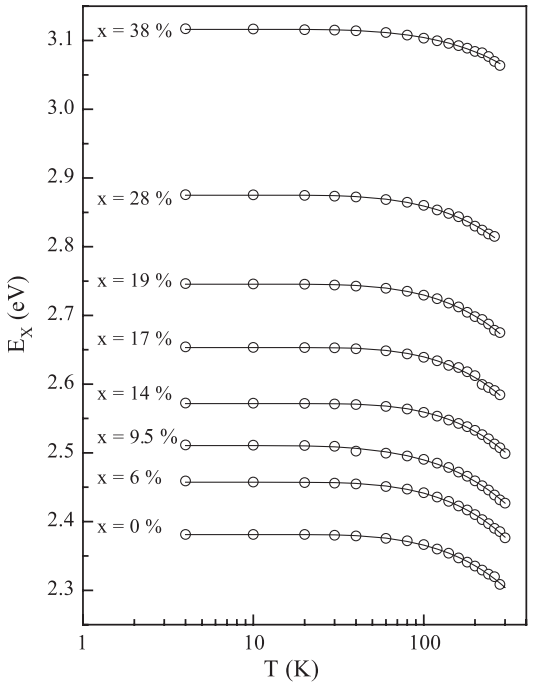

Fig. 5. Temperature dependence of the $Be_xZn_{1-x}Te$ excitonic band gap (E_X). Open symbols are experimental data. The solid lines are theoretical fits to the equation proposed by O'Donnell and Chen [9].

Table 1
Parameters obtained by modeling temperature dependence of band gap energy to the equation by O'Donnell and Chen [9]

Alloy	$E(0)$ (eV)	S	$\langle h\nu \rangle$ (meV)	dE/dT (meV/K)
ZnTe	2.381	1.88±0.04	11.5±0.9	0.32
$Be_{0.06}Zn_{0.94}Te$	2.489	1.96±0.03	11.6±0.6	0.34
$Be_{0.09}Zn_{0.91}Te$	2.547	1.95±0.07	10.9±1.2	0.34
$Be_{0.14}Zn_{0.86}Te$	2.628	1.82±0.04	14.1±0.8	0.31
$Be_{0.17}Zn_{0.83}Te$	2.680	1.94±0.08	13.7±1.5	0.34
$Be_{0.195}Zn_{0.805}Te$	2.725	1.9±0.04	11.3±0.8	0.32
$Be_{0.28}Zn_{0.72}Te$	2.880	1.74±0.04	10.1±0.8	0.30
$Be_{0.38}Zn_{0.62}Te$	3.056	1.27±0.05	9.6±1.5	0.22
ZnTe [10]	2.390	2.29	10.8	0.39
CdTe [10]	1.608	1.68	5.8	0.28
ZnSe [10]	2.818	3.12	15.1	0.54
CdSe [10]	1.764	2.83	18.9	0.49
ZnS [10]	3.836	2.82	16.1	0.49
InP [17]	1.418	1.94	16.8	0.33
h-CdS [24]	2.54	2.33		0.4
h-GaN [25][a]	3.49	2.49		0.43

[a] A-exciton for a free-standing film.

excitonic absorption energy to the semi-empirical equation proposed by O'Donnell and Chen (solid lines):

$$E(T) = E(0) - S(h\nu)[\coth(\langle h\nu \rangle / 2k_BT) - 1] \quad (5)$$

where $E(0)$ is transition energy at 0 K, $h\nu$ is an average phonon energy, and S is a dimensionless electron–phonon coupling constant. Fitting parameters are summarized in Table 1. This model has been previously shown to work well for II–VI ($Zn_{1-x}Mn_xTe$, $Zn_{1-x}Cd_xTe$), III–V ($InAs_xP_{1-x}$), and other semiconductor alloys (GaTe, PbI_2) [15–19].

The data for ZnTe epilayer were also fit to a commonly used relationship proposed by Viña et al. [20]:

$$E_{BE}(T) = E(0) - 2a_B/(e^{\theta/T} - 1) \quad (6)$$

where $E(0)$ is the fundamental transition energy at 0 K, a_B represents the strength of the electron–average phonon interaction, and θ corresponds to the average phonon temperature. Here, the band gap shift is proportional to the sum of the Bose–Einstein statistical factors for phonon emission and absorption. The best fit gives E_0=2.381 eV, a_B=11±1 meV and θ=134±11 K for ZnTe.

The results of the fits to the equations proposed by O'Donnell and Chen and Viña et al. are compared in the high temperature limit where they reduce to:

$$E(T) = E(0) - 2Sk_BT \quad (7)$$

$$E_{BE}(T) = E(0) - 2a_BT/\theta \quad (8)$$

From the given above equations, it follows that:

$$S = a_B/k_B\theta \quad (9)$$

By substituting the values of a_B and θ obtained from the fit to the Bose–Einstein type equation, we calculate S=1.91, in a

good agreement with the value obtained from the relationship by O'Donnell and Chen (S=1.88±0.04), indicating consistency between the parameters obtained by two techniques. Using Eq. (9), we calculate electron–phonon coupling constants for some of the important wide band alloys (Table 1).

From Eq. (7), it follows that temperature band gap variation (dE/dT) is proportional to $-2Sk_B$ at high temperatures (Table 1). From Table 1, it is evident that average phonon energy is constant over the studied compositional range. Electron–phonon coupling constant and temperature band gap variation are nearly constant when the BeTe content is small (x<20%) and start to decrease with higher BeTe content.

Beryllium chalcogenides are known for the lattice hardening properties [21]. For example, increase in the Young's modulus and c_{11} elastic modulus was reported for $Be_xZn_{1-x}Se$ alloy with the increase of BeSe content [22,23]. The dilation lattice contribution to the band gap temperature dependence is described by an equation [9]:

$$\Delta E_{\text{lattice}} = -[(c_{11} + 2c_{12})/3][dE/dP]_v(\Delta V(T)/V_0) \qquad (10)$$

where $[dE/dP]_v$ is the pressure dependence, c_{11} and c_{12} are the elastic moduli, V_0 and $\Delta V(T)$ are the lattice volume and its change with temperature, respectively. Thus, we propose that expected increase in the lattice hardness of $Be_xZn_{1-x}Te$ alloy is responsible for the decrease in the temperature dependence. From Table 1, it is also evident that temperature dependence of $Be_xZn_{1-x}Te$ band gap is smaller compared to other wide band gap semiconductors. This is preferable for device application since unavoidable heating will not cause significant band gap renormalization and will less effect device performance.

4. Conclusion

Optical properties of $Be_xZn_{1-x}Te$ alloys are studied by PL and reflectance measurements. The broadening of exciton emission lines with increase in BeTe content is observed and explained by increase in alloy disorder. The temperature dependence of $Be_xZn_{1-x}Te$ band gap is measured and the data are fit to the formula proposed by O'Donnell and Chen. Average phonon energy and electron–phonon coupling interaction are extracted and studied as a function of BeTe content. Average phonon energy is nearly constant, while electron–phonon coupling constant is smaller for the films with high BeTe content. Temperature dependence of $Be_xZn_{1-x}Te$ band gap is decreasing with the increase in BeTe content and is smaller compared to other wide band gap semiconductors, making it preferable alloy for device application.

References

[1] M.W. Cho, S.K. Hong, J.H. Chang, S. Saeki, M. Nakajima, T. Yao, J. Cryst. Growth 214 (2000) 487.
[2] S.B. Che, I. Nomura, W. Shinozaki, A. Kikuchi, K. Shimomura, K. Kishino, J. Cryst. Growth 214 (2000) 321.
[3] S.B. Che, I. Nomura, A. Kikuchi, K. Kishino, Appl. Phys. Lett. 81 (2002) 972.
[4] S. Nakamura, M. Senoh, S. Nagahama, N. Iwasa, T. Matsushita, T. Mukai, Appl. Phys. Lett. 76 (2000) 22.
[5] A. Kikuchi, K. Kishino, Y. Kanaeko, Jpn. J. Appl. Phys. 30 (1991) 3865.
[6] O. Maksimov, M.C. Tamargo, Appl. Phys. Lett. 79 (2001) 782.
[7] M.R. Buckley, F.C. Peiris, O. Maksimov, M. Muñoz, M.C. Tamargo, Appl. Phys. Lett. 81 (2002) 5156.
[8] M. Muñoz, O. Maksimov, M.C. Tamargo, M.R. Buckley, F.C. Peiris, Phys. Status Solidi, C 1 (2004) (DOI: 10.1002/pssc.200304299).
[9] K.P. O'Donnell, X. Chen, Appl. Phys. Lett. 58 (1991) 2924.
[10] M.W. Cho, J.H. Chang, S. Saeki, S.Q. Wang, T. Yao, J. Vac. Sci. Techol., B 18 (2000) 457.
[11] I. Hernandez-Calderon, in: M.C. Tamargo (Ed.), II–VI Semiconductor Materials and Their Applications, Taylor and Franics, New York, 2002, and references there in.
[12] V. Bousquet, E. Tournie, J.P. Fourie, J. Cryst. Growth 192 (1998) 102.
[13] V. Wagner, S. Gundel, J. Geurts, T. Gerhard, Th. Litz, H.J. Lugauer, F. Fischer, A. Waag, G. Landwehr, R. Kurse, Ch. Becker, U. Küster, J. Cryst. Growth 184 (1998) 1067.
[14] E.F. Schubert, E.O. Göbel, Y. Horikosi, K. Ploog, H.J. Queisser, Phys. Rev., B 30 (1984) 813.
[15] Y.T. Shih, W.C. Chiang, C.S. Yang, M.C. Kuo, W.C. Chou, J. Appl. Phys. 92 (2002) 2446.
[16] Y.T. Shih, W.C. Fan, C.S. Yang, M.C. Kuo, W.C. Chou, J. Appl. Phys. 94 (2003) 3791.
[17] M. Wada, S. Araki, T. Kudou, T. Umezawa, S. Nakajima, Appl. Phys. Lett. 76 (2000) 2722.
[18] A. Zubiaja, J.A. Garcia, F. Plazaola, V. Muñoz-Sanjose, M.C. Martinez-Tomas, J. Appl. Phys. 92 (2002) 7330.
[19] R. Ahuja, H. Arwin, A. Ferreira da Silva, C. Persson, J.M. Osorio-Guillén, J. Souza de Almeida, C. Moyses Araujo, E. Veje, N. Veissid, C.Y. An, I. Pepe, B. Johansson, J. Appl. Phys. 92 (2002) 7219.
[20] L. Viña, S. Logothetidis, M. Cardona, Phys. Rev., B 30 (1984) 1979.
[21] C. Verie, in: B. Gil, R.L. Aulombard (Eds.), Semiconductor Heteroepitaxy, World Scientific, Singapore, 1995.
[22] S.E. Grillo, M. Dicarroir, M. Nadal, E. Tournie, J.P. Faurie, J. Phys., D 35 (2002) 3015.
[23] F.C. Peiris, U. Bindley, J.K. Furdyna, H. Kim, A.K. Ramdas, M. Grimsditch, Appl. Phys. Lett. 79 (2001) 473.
[24] G. Perna, V. Capozzi, S. Pagliora, M. Ambricio, D. Lojacono, Thin Solid Films 387 (2001) 208.
[25] Y.S. Huang, F.H. Pollak, S.S. Park, K.Y. Lee, H. Morkoç, J. Appl. Phys. 94 (2003) 899.